Exposed hydrophobicity is a key determinant of nuclear quality control degradation

Eric K. Fredrickson*, Joel C. Rosenbaum*, Melissa N. Locke, Thomas I. Milac, and Richard G. Gardner
Department of Pharmacology, University of Washington, Seattle, WA 98195

ABSTRACT Protein quality control (PQC) degradation protects the cell by preventing the toxic accumulation of misfolded proteins. In eukaryotes, PQC degradation is primarily achieved by ubiquitin ligases that attach ubiquitin to misfolded proteins for proteasome degradation. To function effectively, PQC ubiquitin ligases must distinguish misfolded proteins from their normal counterparts by recognizing an attribute of structural abnormality commonly shared among misfolded proteins. However, the nature of the structurally abnormal feature recognized by most PQC ubiquitin ligases is unknown. Here we demonstrate that the yeast nuclear PQC ubiquitin ligase San1 recognizes exposed hydrophobicity in its substrates. San1 recognition is triggered by exposure of as few as five contiguous hydrophobic residues, which defines the minimum window of hydrophobicity required for San1 targeting. We also find that the exposed hydrophobicity recognized by San1 can cause aggregation and cellular toxicity, underscoring the fundamental protective role for San1-mediated PQC degradation of misfolded nuclear proteins.

INTRODUCTION

Cellular proteins are exposed to numerous chemical and physical hazards, such as reactive oxygen species and heat shock, that can damage their structural integrity and cause misfolding. Even under optimal physiological conditions, the cell is faced with the continuous stochastic production of misfolded proteins through synthesis errors, which can threaten cell viability if they are not managed appropriately. The deleterious consequences of not dealing with misfolded proteins properly are highlighted by the many human disorders that result from protein aggregation, for example, Alzheimer, Parkinson, and Huntington disorders and amyotrophic lateral sclerosis (Ross and Poirier, 2005).

One key way in which the cell manages misfolded proteins is by destroying them through protein quality control (PQC) degradation. In eukaryotes, PQC degradation occurs principally through compartment-specific ubiquitin ligases that target misfolded proteins for ubiquitination and subsequent destruction by the proteasome (McDonough and Patterson, 2003; Mijaljica et al., 2007; Vembar and Brodsky, 2008). Ubiquitin ligases typically determine substrate specificity in ubiquitination pathways, and those ligases involved in PQC must be able to discriminate misfolded proteins from their normally folded counterparts to function effectively. Without this critical capacity, PQC degradation systems would subject structurally intact normal proteins to random destruction. Because any protein could lose its structure and become misfolded, PQC ubiquitin ligases must also be able to recognize a diverse assortment of unrelated substrates by targeting a common feature of structural abnormality. We understand poorly what structurally abnormal features PQC ubiquitin ligases recognize in their misfolded substrates.

Ubiquitin ligases that function in PQC degradation have been identified in the endoplasmic reticulum (ER) (Hampton et al., 1996; Bordallo et al., 1998; Fang et al., 2001; Swanson et al., 2001; Kaneko et al., 2002; Nadav et al., 2003), cytoplasm (Jiang et al., 2001; Murata et al., 2001; Heck et al., 2010; Nillegoda et al., 2010), and nucleus (Fu et al., 2005; Gardner et al., 2005; Janer et al., 2006; Iwata et al., 2009; Wang and Prelich, 2009). Of these known PQC

ubiquitin ligases, the ER membrane–bound PQC ubiquitin ligases Hrd1 and Doa10 in budding yeast have been the most extensively studied, and we now have some information on the structurally abnormal features these ligases might recognize in their substrates. Misfolded proteins that present their folding lesions in the ER lumen are targeted by Hrd1 (Vashist and Ng, 2004; Carvalho et al., 2006), which uses various ER lumen adaptor proteins, including its partner Hrd3 (SEL1L in mammals), the Hsp70 chaperone Kar2/BiP, and the lectin Yos9 (OS-9 and XTP3-B in mammals), to target misfolded ER lumen proteins (Brodsky et al., 1999; Gardner et al., 2000; Vashist et al., 2001; Taxis et al., 2003; Buschhorn et al., 2004; Vashist and Ng, 2004; Bhamidipati et al., 2005; Kim et al., 2005; Carvalho et al., 2006; Denic et al., 2006; Gauss et al., 2006; Mueller et al., 2006; Hosokawa et al., 2007; Christianson et al., 2008; Kanehara et al., 2010). For misfolded glycoproteins in the ER lumen, the Hrd1 complex uses Yos9 to recognize specific N-linked glycan moieties in the misfolded substrate (Bhamidipati et al., 2005; Kim et al., 2005; Quan et al., 2008; Clerc et al., 2009), and these appear to be located near unstructured segments of the misfolded protein (Xie et al., 2009). What Hrd1 recognizes in misfolded ER lumen proteins that lack glycan moieties is not known. The Hrd1-dependent degradation of nonglycosylated misfolded proteins requires the Hsp70 chaperone Kar2/BiP (Kanehara et al., 2010), which could suggest that the Hrd1 pathway (through interaction with substrate-bound chaperones) targets hydrophobic residues that are normally buried in the folded protein's core but have become surface exposed through misfolding. In addition to Hrd1's role in targeting misfolded ER lumen proteins, Hrd1 also recognizes misfolded ER membrane proteins (Hampton et al., 1996; Bordallo et al., 1998; Carvalho et al., 2006; Sato et al., 2009). For these cases, it appears that Hrd1 uses its transmembrane domain to sense folding lesions in misfolded ER transmembrane domains, perhaps by recognizing hydrophilic residues exposed in the hydrophobic environment of the membrane (Sato et al., 2009).

In contrast to Hrd1, Doa10 recognizes misfolded ER proteins that present their folding lesions on the cytoplasmic side of the ER membrane (Swanson et al., 2001; Huyer et al., 2004; Carvalho et al., 2006; Nakatsukasa et al., 2008). Doa10 likely recognizes exposed hydrophobicity in its misfolded substrates, as numerous studies have identified synthetic hydrophobic peptides that cause Doa10 pathway–dependent degradation of attached reporters (Sadis et al., 1995; Gilon et al., 2000; Ravid et al., 2006; Metzger et al., 2008). Furthermore, the transcription factor MATα2 is also targeted for Doa10-dependent degradation, with Doa10 recognizing the exposed hydrophobic face of an amphipathic helix normally buried when MATα2 forms a heterodimer with MATa1 (Johnson et al., 1998; Ravid et al., 2006). Because cytoplasmic chaperones are involved in the degradation of many Doa10 substrates (Huyer et al., 2004; Metzger et al., 2008; Nakatsukasa et al., 2008), it is possible that Doa10 targets exposed hydrophobicity in misfolded proteins through the action of cytoplasmic chaperones, similar to how Hrd1 might use ER lumen chaperones.

It is important to consider that the abnormal features targeted by PQC ubiquitin ligases might differ depending on the cellular compartment. For example, the ER and cytoplasm are sites of initial protein synthesis, and PQC degradation systems in these compartments must avoid targeting nascent proteins in the process of folding normally but still be capable of recognizing both nascent proteins that fold abnormally and normally folded proteins that have become misfolded through damage. With this constraint, PQC ubiquitin ligases in the ER and cytoplasm likely operate via a triage mechanism involving chaperones in the initial decision-making step
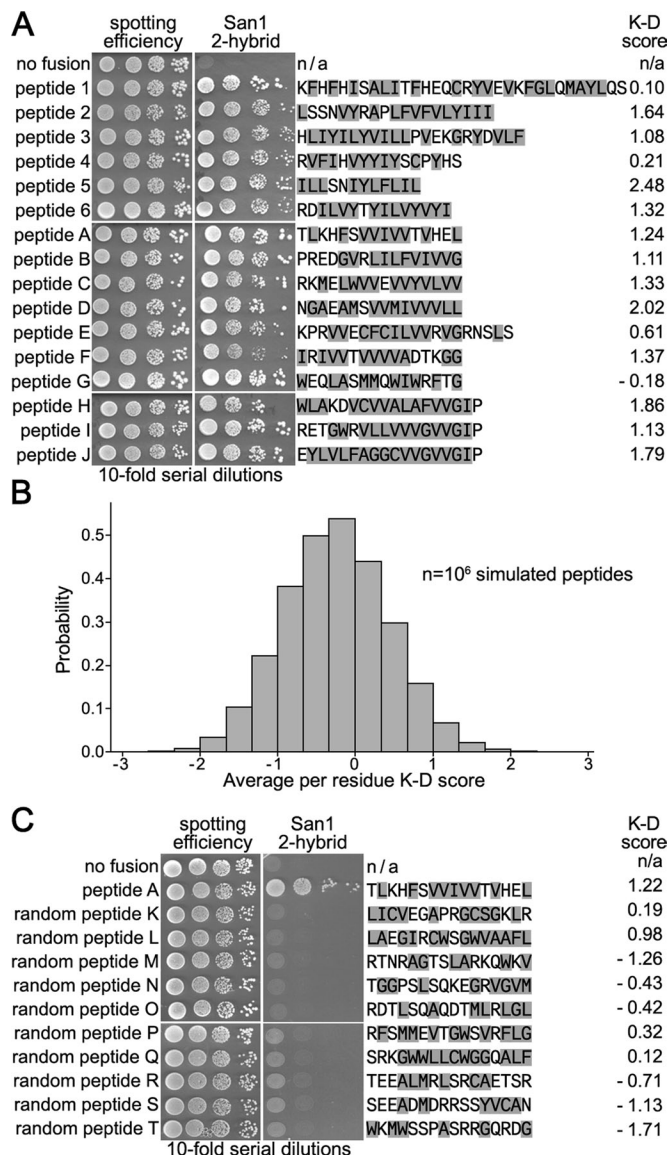
in PQC degradation (Wickner et al., 1999; McClellan et al., 2005). On the other hand, the nucleus is a posttranslational compartment where little, if any, protein biosynthesis occurs. Thus nuclear PQC degradation systems need not be constrained by nascent protein folding. Whether PQC degradation systems in the nucleus operate under similar or different rules of substrate recognition and detection than PQC degradation systems in the ER and cytoplasm is not known. To address this, we focused our efforts on understanding how the yeast nuclear PQC ubiquitin ligase San1 functions in substrate targeting. San1 ubiquitinates misfolded nuclear proteins for proteasome degradation (Dasgupta et al., 2004; Gardner et al., 2005) by binding its misfolded substrates using intrinsically disordered domains (Rosenbaum et al., 2011). Here we report that San1 recognizes a small window of exposed hydrophobicity across a spectrum of different misfolded nuclear substrates.

RESULTS

Under normal physiological conditions, PQC degradation systems typically target only a small, random portion of an individual protein's total pool that has become misfolded through synthesis errors or postsynthesis damage or has failed to complex correctly with its partner proteins. Because of the difficulties in examining a small portion of any protein's pool, PQC degradation studies have routinely used three different types of substrates whose entire pool can be induced to misfold. The first type of PQC substrate comprises synthetic peptides, which when fused to reporter proteins can cause their PQC ubiquitin ligase–dependent degradation (Gilon et al., 1998, 2000; Metzger et al., 2008). It is thought that synthetic peptides mimic some feature present in misfolded proteins that is typically recognized by PQC ubiquitin ligases. The second type of PQC substrate consists of truncated proteins (Ward et al., 1995; Park et al., 2007; Heck et al., 2010; Rosenbaum et al., 2011). Presumably, truncated proteins cannot fold into a proper structure, and thus they represent constitutively misfolded proteins targeted by PQC ubiquitin ligases. The third type of PQC substrate encompasses missense mutant proteins (Betting and Seufert, 1996; Biederer et al., 1996; Bordallo et al., 1998; Dasgupta et al., 2004; Gardner et al., 2005; Ravid et al., 2006; Kaganovich et al., 2008; Estruch et al., 2009; Lewis and Pelham, 2009; Wang and Prelich, 2009; Matsuo et al., 2011). In these cases, single missense mutations lead to misfolding of a protein and subsequent recognition by PQC ubiquitin ligases. Often the missense mutations cause temperature-dependent loss of protein function that can be recovered by eliminating their PQC degradation (Betting and Seufert, 1996; Bordallo et al., 1998; Dasgupta et al., 2004; Gardner et al., 2005; Ravid et al., 2006; Wang et al., 2006; Estruch et al., 2009), indicating that the misfolding caused by the mutations is not so severe that all protein function is lost. For our studies, we used examples from each different type of substrate to see if we could identify a universal feature of structural abnormality targeted by San1.

Small hydrophobic peptides function as degrons for San1-mediated degradation

We recently identified 29 misfolded substrates that interact with San1, using a two-hybrid genetic selection in which a catalytically inactive version of San1 bearing a C279S mutation in its RING domain was fused to the Gal4 DNA-binding domain (GBD) and a yeast cDNA library that was fused to the Gal4 activation domain (GAD) (Rosenbaum et al., 2011). One interesting class of substrates identified by this analysis was made up of cDNAs oriented in the reverse direction to the GAD, causing the translation of random peptide sequences fused to the GAD rather than the desired protein encoded

A

	spotting efficiency	San1 2-hybrid		K-D score
no fusion			n/a	n/a
peptide 1			KFHFHISALITFHEQCRYVEVKFGLQMAYLQS	0.10
peptide 2			LSSNVYRAPLFVFVLYIII	1.64
peptide 3			HLIYILYVILLPVEKGRYDVLF	1.08
peptide 4			RVFIHVYYIYSCPYHS	0.21
peptide 5			ILLSNIYLFLIL	2.48
peptide 6			RDILVYTYILVYVYI	1.32
peptide A			TLKHFSVVIVVTVHEL	1.24
peptide B			PREDGVRLILFVIVVG	1.11
peptide C			RKMELWVVEVVYVLVV	1.33
peptide D			NGAEAMSVVMIVVVLL	2.02
peptide E			KPRVVECFCILVVRVGRNSLS	0.61
peptide F			IRIVVTVVVVADTKGG	1.37
peptide G			WEQLASMMQWIWRFTG	- 0.18
peptide H			WLAKDVCVVALAFVVGIP	1.86
peptide I			RETGWRVLLVVVGVVGIP	1.13
peptide J			EYLVLFAGGCVVGVVGIP	1.79

10-fold serial dilutions

B

n=10^6 simulated peptides

(y-axis: Probability; x-axis: Average per residue K-D score)

C

	spotting efficiency	San1 2-hybrid		K-D score
no fusion			n/a	n/a
peptide A			TLKHFSVVIVVTVHEL	1.22
random peptide K			LICVEGAPRGCSGKLR	0.19
random peptide L			LAEGIRCWSGWVAAFL	0.98
random peptide M			RTNRAGTSLARKQWKV	- 1.26
random peptide N			TGGPSLSQKEGRVGVM	- 0.43
random peptide O			RDTLSQAQDTMLRLGL	- 0.42
random peptide P			RFSMMEVTGWSVRFLG	0.32
random peptide Q			SRKGWWLLCWGGQALF	0.12
random peptide R			TEEALMRLSRCAETSR	- 0.71
random peptide S			SEEADMDRRSSYVCAN	- 1.13
random peptide T			WKMWSSPASRRGQRDG	- 1.71

10-fold serial dilutions

FIGURE 1: San1 interacts with hydrophobic peptides. (A) Cells expressing GBD-San1^{C279S} and each listed peptide fused to GAD were spotted onto media with or without histidine to measure spotting efficiency and two-hybrid interaction. Hydrophobic residues are in gray. Average K-D scores for each peptide are listed on the right. (B) Histogram of the K-D scores generated from 10^6 simulated peptides selected randomly from the 16-mer peptide library. (C) Cells expressing GBD-San1^{C279S} and the indicated randomly selected peptide were spotted as in A. Hydrophobic residues are in gray.

by the cDNA. Inspection of the peptide sequences revealed that five of the six peptides contain long tracts of hydrophobic residues (Figure 1A, peptides 1–6), suggesting that San1 targets exposed hydrophobicity. To explore this further, we obtained a quantitative measure of peptide hydrophobicity by averaging the Kyte–Doolittle (K-D) hydrophobicity (Kyte and Doolittle, 1982) values for each residue in the peptide, thus yielding an average hydrophobicity score for each peptide (which we call a K-D score). We classified a peptide as hydrophobic if it has a K-D score >0 and as hydrophilic if it has a K-D score <0. All six peptides have K-D scores >0 (Figure 1A).

To determine whether San1 generally binds hydrophobic peptides, we subsequently performed a two-hybrid selection using a library of ~10^7 random 16-mer peptides fused to the GAD (Yang

et al., 1995). We identified 10 unique peptides that interact with San1, and 9 of the 10 have K-D scores >0 (Figure 1A, peptides A–J). The K-D scores again suggested that San1 targets hydrophobicity. To determine the likelihood that this result could occur by chance, we selected at random 10^6 simulated peptides from the library (based on the library's idealized composition) and found that the probability of selecting a peptide with a K-D score >0 is 0.336 (Figure 1B). Therefore it is unlikely that 9 of 10 peptides chosen at random from the library would have K-D scores >0 (P value = 3.8 × 10^{-4}). To verify that the library itself is not biased toward hydrophobicity, we sequenced 10 randomly chosen peptides and found 4 to have K-D scores >0 (Figure 1C, random peptides K–T), indicating that the peptide composition of the library is as expected (P value = 0.448). None of the randomly chosen peptides interacts with San1 by two-hybrid (Figure 1C), which we expected since they were not identified as interactors in the two-hybrid selection.

Recently we found that San1 is an intrinsically disordered protein (IDP) (Rosenbaum *et al.*, 2011). Intrinsic disorder confers conformational flexibility that enables an IDP to interact with a wide variety of structurally diverse proteins. Because of this flexibility, we considered the possibility that the San1-interacting hydrophobic peptides might simply interact with *any* IDP nonspecifically. To test this, we measured the two-hybrid interaction between all peptides and the deubiquitinating enzyme Ubp10, which is as highly disordered outside of its catalytic domain as San1 (Figure 2A). No peptide interacted with Ubp10 (Figure 2B), demonstrating that the interactions of hydrophobic peptides are specific for San1 and ruling out the possibility that they simply interact nonspecifically with any IDP.

We verified that the San1-interacting peptides target reporter fusions for San1-mediated degradation by attaching the peptides to green fluorescent protein (GFP) containing a nuclear localization signal (NLS), which allowed us to target the GFP fusions to the nucleus where San1 resides (Gardner *et al.*, 2005). We analyzed the degradation of the GFP^{NLS}-peptide fusions in mutant *san1Δ* and wild-type *SAN1* cells using a cycloheximide-chase assay, which measures protein degradation after synthesis is blocked. Each GFP^{NLS}-peptide is rapidly degraded in wild-type *SAN1* cells and stabilized in mutant *san1Δ* cells (see representative examples in Figure 3A), which is consistent with their interactions with San1 in the two-hybrid assay (Figure 1A). By contrast, the randomly selected peptides, which do not interact with San1 in the two-hybrid assay (Figure 1B), are not subject to San1-dependent degradation; the GFP^{NLS}-random peptide fusions are either stable or degraded in a San1-independent manner (see representative examples in Figure 3B). Because the San1-interacting, cDNA-derived peptides have stretches of hydrophobic residues and hydrophilic residues, we confirmed that the hydrophobic residues are solely responsible for San1-dependent degradation by splitting peptides 2 and 3 into their constituent hydrophobic and hydrophilic parts. We observed San1-dependent degradation only when the hydrophobic, but not the hydrophilic, part of these peptides is fused to GFP^{NLS} (Figure 3, C and D).

A few of the randomly selected peptides do not interact with San1 but do have K-D scores >0 (Figure 1C), so it is likely that San1 recognizes something other than the overall hydrophobicity of the peptide. We hypothesized that San1 recognizes regions within each peptide in which hydrophobic residues are concentrated and hydrophobicity predominates. To test this, we determined the minimum number of contiguous hydrophobic residues required for San1-dependent degradation by substituting an increasing number of serine or threonine residues for the N-terminal hydrophobic residues in the peptide 2 and 3 hydrophobic variants. We found that San1 requires a minimum of five contiguous hydrophobic residues
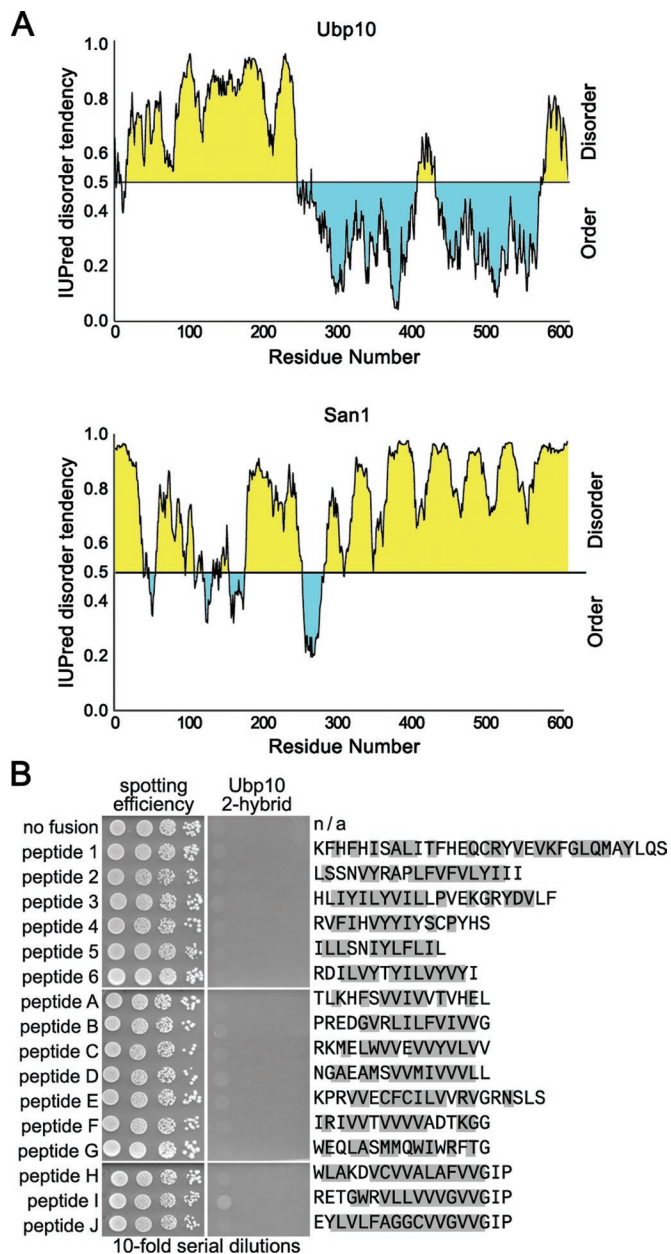
FIGURE 2: San1-interacting peptides do not interact with a similarly disordered protein. (A) Disorder predictions of Ubp10 and San1. Panels were generated from IUPred (http://iupred.enzim.hu/index .html). Predicted disordered regions are in yellow, and predicted ordered regions are in blue. (B) Cells expressing GBD-Ubp10 and each listed peptide fused to GAD were spotted onto media with or without histidine to measure spotting efficiency and two-hybrid interaction. Hydrophobic residues are in gray.

to target the GFP^{NLS}-peptides for degradation (Figure 3, C and D). Consistent with the idea that a window of hydrophobicity rather than overall hydrophobicity is recognized by San1, we found that the peptide 2 and 3 variants with only four contiguous hydrophobic residues are not degraded despite the fact that they have overall K-D scores >0 (TSTSTSYIII, 0.77; TSTSTSVILL, 1.18). Thus we conclude that a local window of concentrated hydrophobicity rather than overall peptide hydrophobicity is the primary determinant of San1 recognition.
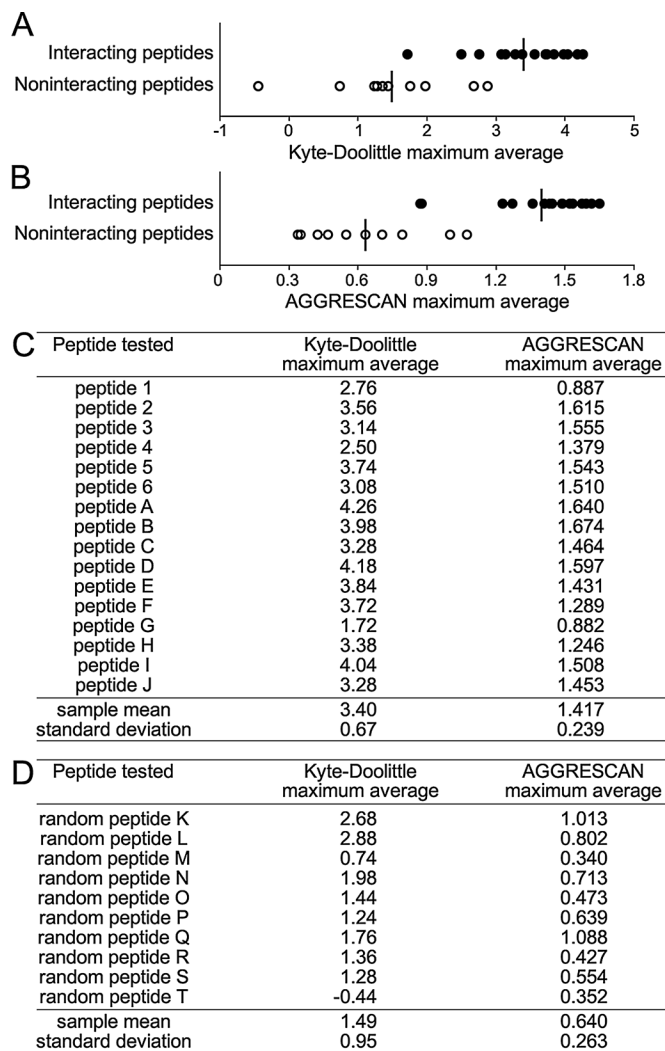
To examine the "window of hydrophobicity" hypothesis further, we evaluated the local K-D hydrophobicity score in a five-residue
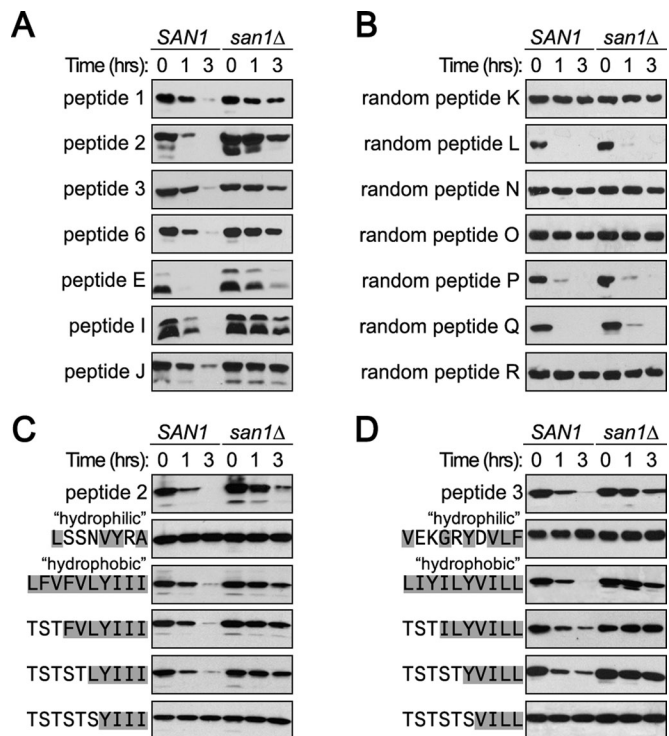
FIGURE 3: Hydrophobic peptides are degraded in a San1-dependent manner. Cycloheximide-chase assays were performed to assess stability of the indicated GFP^{NLS}-peptide fusion in the presence or absence of *SAN1*. Time after cycloheximide addition is indicated. (A) Examples of the degradation of GFP^{NLS}-interacting peptide fusions. (B) Examples of the degradation of GFP^{NLS}-randomly selected peptide fusions. (C) Degradation assays of peptide 2 hydrophilic and hydrophobic variants. (D) Degradation assays of peptide 3 hydrophilic and hydrophobic variants.

sliding window across the length of all San1-interacting and noninteracting peptides. We recorded the maximum five-residue window value found for each peptide and plotted the values of San1-interacting and noninteracting peptides separately for comparison (Figure 4, A, C, and D). We observed a significantly higher mean K-D window value for the San1-interacting peptides compared with that for the noninteracting randomly selected peptides (P value = 2.9×10^{-5}). The K-D value has particular biases in characterizing hydrophobicity (Kyte and Doolittle, 1982), so we also evaluated the maximum hydrophobicity window value in all peptides using AGGRESCAN, an algorithm trained to predict the aggregation propensity of protein regions based on their residues' hydrophobic content (Conchillo-Sole *et al.*, 2007). We found that the San1-interacting peptides also have higher maximum AGGRESCAN window values than their noninteracting counterparts (Figure 4, B–D), with even greater statistical separation of the mean values (P value = 2.8×10^{-7}). Altogether, the experimental evidence coupled with the hydrophobicity analyses indicates that San1 recognizes a window of concentrated hydrophobicity in its target peptides.

Although there is a significant correlation between the window of hydrophobicity in a peptide and its interaction with San1 and San1-dependent degradation, there are some interesting outliers that cannot be explained solely by this simple model. Both peptides 1 and G interact with San1 and are degraded in a San1-dependent manner, but each has significantly lower K-D and AGGRESCAN maximum window averages than the other interacting peptides. Conversely,

C	Peptide tested	Kyte-Doolittle maximum average	AGGRESCAN maximum average
	peptide 1	2.76	0.887
	peptide 2	3.56	1.615
	peptide 3	3.14	1.555
	peptide 4	2.50	1.379
	peptide 5	3.74	1.543
	peptide 6	3.08	1.510
	peptide A	4.26	1.640
	peptide B	3.98	1.674
	peptide C	3.28	1.464
	peptide D	4.18	1.597
	peptide E	3.84	1.431
	peptide F	3.72	1.289
	peptide G	1.72	0.882
	peptide H	3.38	1.246
	peptide I	4.04	1.508
	peptide J	3.28	1.453
	sample mean	3.40	1.417
	standard deviation	0.67	0.239

D	Peptide tested	Kyte-Doolittle maximum average	AGGRESCAN maximum average
	random peptide K	2.68	1.013
	random peptide L	2.88	0.802
	random peptide M	0.74	0.340
	random peptide N	1.98	0.713
	random peptide O	1.44	0.473
	random peptide P	1.24	0.639
	random peptide Q	1.76	1.088
	random peptide R	1.36	0.427
	random peptide S	1.28	0.554
	random peptide T	-0.44	0.352
	sample mean	1.49	0.640
	standard deviation	0.95	0.263

FIGURE 4: San1-interacting peptides are defined by a local window of hydrophobicity. (A) A K-D sliding scale of five residues was used to determine the maximum hydrophobic window in San1-interacting (●) and noninteracting (○) peptides. Vertical line marks the mean of each group. (B) Using AGGRESCAN values, a sliding-scale analysis was performed as in A. (C, D) The maximum hydrophobic window value using K-D and AGGRESCAN is listed for each interacting peptide (C) and randomly selected noninteracting peptide (D).

random peptides L and Q have maximum window averages that resemble those of San1-interacting peptides. However, these peptides do not interact with San1 and are subject to San1-independent degradation. See the *Discussion* for the potential reasons why we think these outliers are consistent with the "window of hydrophobicity" model of San1 recognition.

San1 targets hydrophobicity in truncated substrates

The hydrophobicity that San1 recognizes in the peptides likely reflects a similar feature that San1 targets in the misfolded proteins it typically encounters in the nucleus. To see whether this is the case, we turned to the other San1 substrates that we previously discovered in the two-hybrid cDNA selection (Rosenbaum *et al.*, 2011), which are predominantly truncated proteins fused to the NLS-containing GAD. For these substrates, we hypothesized that the truncations cause hydrophobic regions normally buried in the full-length

protein to become surface exposed and accessible to San1 when they are localized to the nucleus by virtue of their fusion to the GAD. We identified candidate hydrophobic regions in each truncated substrate by plotting K-D hydrophobicity values along their sequence lengths (Supplemental Figure S1). Fifteen truncated substrates have multiple hydrophobic stretches scattered throughout the protein; we categorized these as group I substrates. Six truncated substrates contain only a single pronounced stretch of hydrophobicity; we categorized these as group II substrates.

To determine whether San1 recognizes hydrophobicity in truncated substrates, we focused our attention on members of group II due to the simplicity of their hydrophobicity profiles. The group II substrate Rad16* is a mutant form of the nuclear excision repair protein Rad16 in which residues 116–664 have been deleted. Rad16* possesses a 28-residue hydrophobic patch spanning residues 142–169 in the truncated Rad16* protein (Figure 5A). This region corresponds to residues 691–718 in full-length Rad16 that normally would have been buried. Another group II substrate is Sed1*, which is a mutant form of the cell wall protein Sed1 in which the first 20 residues have been deleted. The truncated Sed1* protein contains a hydrophobic region spanning its final 44 residues (Figure 5A). The hydrophobic patches in both Rad16* and Sed1* each contain a maximum five-residue hydrophobic window with values similar to the San1-interacting peptides (Figure 5B), making them the likely regions recognized by San1 when localized to the nucleus. Both Rad16* and Sed1* interact with San1 in the two-hybrid assay (Figure 5C) and undergo San1-dependent degradation (Figure 5D). Deletion of the hydrophobic patch in Rad16* and Sed1* disrupts their interaction with San1 (Figure 5C, GAD-Rad16*[Δh] and -Sed1*[Δh]) and eliminates their San1-dependent degradation (Figure 5D). Conversely, the isolated hydrophobic patch from Rad16* (residues 691–718 of full-length Rad16) and Sed1* (residues 294–338 in full-length Sed1) is sufficient to cause interaction with San1 (Figure 5C, GAD-Rad16*[hydro only] and -Sed1*[hydro only]) and induce San1-dependent degradation (Figure 5D). On the basis of these results, we conclude that San1 also recognizes a window of exposed hydrophobicity in its truncated substrates.

Missense mutant San1 substrates have increased surface hydrophobicity

In addition to the peptides and truncated proteins, San1 also targets six different proteins containing single missense mutations for degradation: Sir4-9, Cdc68-1, Sir3-8, Cdc13-1, Mex67-5, Ura3-2 and Ura3-3 (Evans *et al.*, 1998; Dasgupta *et al.*, 2004; Gardner *et al.*, 2005; Estruch *et al.*, 2009; Lewis and Pelham, 2009). Most missense mutant proteins degraded via San1 retain a significant portion of wild-type function after elimination of their PQC degradation by deletion of San1 (Schnell *et al.*, 1989; Xu *et al.*, 1993; Gardner *et al.*, 2005; Addinall *et al.*, 2008; Estruch *et al.*, 2009; Lewis and Pelham, 2009), suggesting that the functional structure of the mutant proteins is largely intact. In these cases, we hypothesized that the mutation causes a local misfolding that exposes normally buried hydrophobic residues in a part of the protein not primarily involved in the protein's function.

To test this hypothesis, we wanted to measure the surface hydrophobicity of missense mutant San1 substrates to see whether the mutant versions had increased exposed hydrophobicity compared with their wild-type counterpart. For this analysis, we focused on missense mutant San1 substrates that have a crystal structure solved for the wild-type protein because we reasoned that these should be the best behaved during purification from bacteria and use in vitro. The yeast protein Ura3 has a known crystal structure (Chan *et al.*,
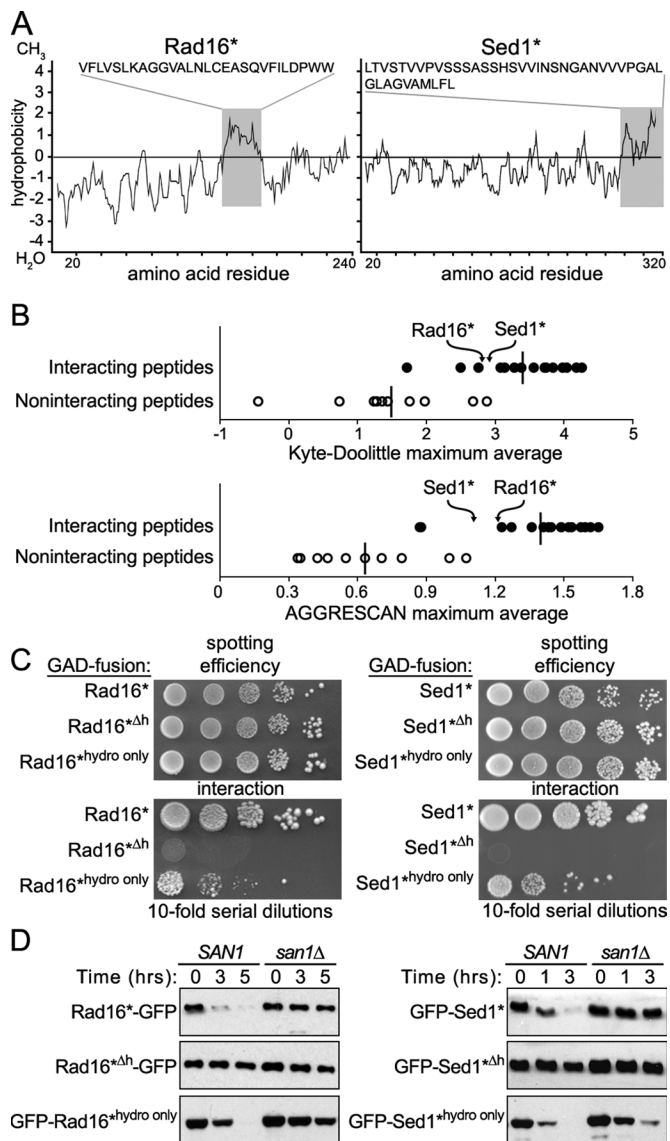
FIGURE 5: Hydrophobic regions in truncated proteins are necessary and sufficient for interaction with and degradation via San1. (A) K-D plots of Rad16* and Sed1* hydrophobicity. Gray indicates a stretch of hydrophobicity. The amino acid sequence of Rad16* and Sed1* in the gray box is indicated. (B) K-D and AGGRESCAN sliding-scale analyses were performed to determine the maximum average hydrophobic window in the hydrophobic stretches of Rad16* and Sed1*. (C) Cells expressing GBD-San1 and the indicated GAD-Rad16* and GAD-Sed1* fusions were spotted onto media with or without histidine to measure spotting efficiency and two-hybrid interaction. (D) Cycloheximide-chase assays were performed to assess the stability of the indicated GFP-Rad16* and GFP[NLS]-Sed1*.

2009) and two mutants, Ura3-2 (P144L) and Ura3-3 (D243G), that are subject to San1-mediated degradation (Lewis and Pelham, 2009). Each wild-type Ura3 residue that is mutated is positioned near hydrophobic regions of at least five residues long buried in the structure (Figure 6, A and B): P144 is positioned near regions 84–89 (YNFLLF), 146–151 (GLLMLA), and 178–184 (FVIGFIA), whereas D243 is positioned near regions 197–206 (WLIMTPGVGL) and 230–234 (IIIVG). When we examined the sequence of Ura3 using the K-D or AGGRESCAN sliding window measures, we found that these local hydrophobic regions possess a maximum hydrophobicity window value comparable to the values in the San1-interacting peptides and truncated proteins (Figure 6, C and D).

We purified Ura3, Ura3-2, and Ura3-3 from *Escherichia coli* and examined their surface hydrophobicity by measuring their ability to bind the dye 1-anilinonaphthalene-8-sulfonate (ANS) in vitro. ANS is negligibly fluorescent in an aqueous environment but binds hydrophobic residues and fluoresces in a hydrophobic environment (Hawe et al., 2008). ANS incubated with mutant Ura3-2 and Ura3-3 produced a fluorescence signal significantly brighter than seen with normal Ura3 (Figure 6E), indicating greater surface exposed hydrophobicity in the mutants. This result correlates with the San1-dependent degradation of Ura3-2 and Ura3-3 in vivo (Figure 6F) and is consistent with the hypothesis that San1 also targets exposed hydrophobicity in this type of substrate.

Although it is difficult to ascertain how a missense mutation causes misfolding by sequence and position alone (Gianni et al., 2010), we hypothesized that the misfolding might be proximal to the mutation. Therefore we focused our attention on the proximal hydrophobic regions located near each residue mutated in the Ura3 structure. We examined whether these mutation-proximal hydrophobic regions could function as San1 degrons in vivo by fusing 16-mer peptides containing the five highest maximum Ura3 hydrophobic windows (as described earlier) to GFP[NLS] and testing for San1-dependent degradation. We chose peptides with lengths of 16 residues so that the experiment is consistent with the peptide lengths used in Figure 1. Only the GFP[NLS] fusions with the Ura3 peptides spanning residues 140–155 and 226–241, the most proximal to each mutated residue (P144 and D243), are degraded in wild-type *SAN1* cells (Figure 6G). Each is partially stabilized in the absence of *SAN1* (Figure 6G), indicating that San1 can recognize these regions if they become exposed.

Because the peptide 226–241 was competent for San1-dependent degradation when fused to GFP[NLS], we decided to see whether we could mutate this region near the D243G mutation to reduce the hydrophobicity in Ura3-3. Unfortunately, when we mutated the hydrophobic residues proximal to the Ura3-3 mutation (I231 and V233), we found the additionally mutated Ura3-3[I231A, V232A] protein was now subject to primarily San1-independent PQC degradation (Figure 6H), thus hindering our ability to test the exposed hydrophobicity model in Ura3-3 further. This was not unexpected, however, in that additional mutations to hydrophobic residues could cause further misfolding that now reveals features of structural abnormality recognized by other PQC degradation systems. Despite our inability to test the hypothesis in full-length Ura3-2 and Ura3-3 by mutational analyses, the rest of the data are consistent with San1 recognizing exposed hydrophobicity in missense mutant substrates.

Exposed hydrophobicity targeted by San1 can lead to aggregation and nuclear toxicity

From an evolutionary perspective, San1 likely evolved to recognize a feature of structural abnormality that has negative consequences if allowed to persist in the cell. Misfolded proteins tend to aggregate due to the interaction of inappropriately exposed hydrophobic surfaces (Chiti, 2006). Protein aggregation can have deleterious effects on cell viability, as evidenced by the many known protein aggregation disorders (Skovronsky et al., 2006). We recently found that expression of 11 different San1 substrates in *san1Δ* cells is toxic and affects cell viability (Rosenbaum et al., 2011). Because San1 targets hydrophobicity, we reasoned that aggregation resulting from exposed hydrophobicity in these substrates is likely responsible for their toxic effects.
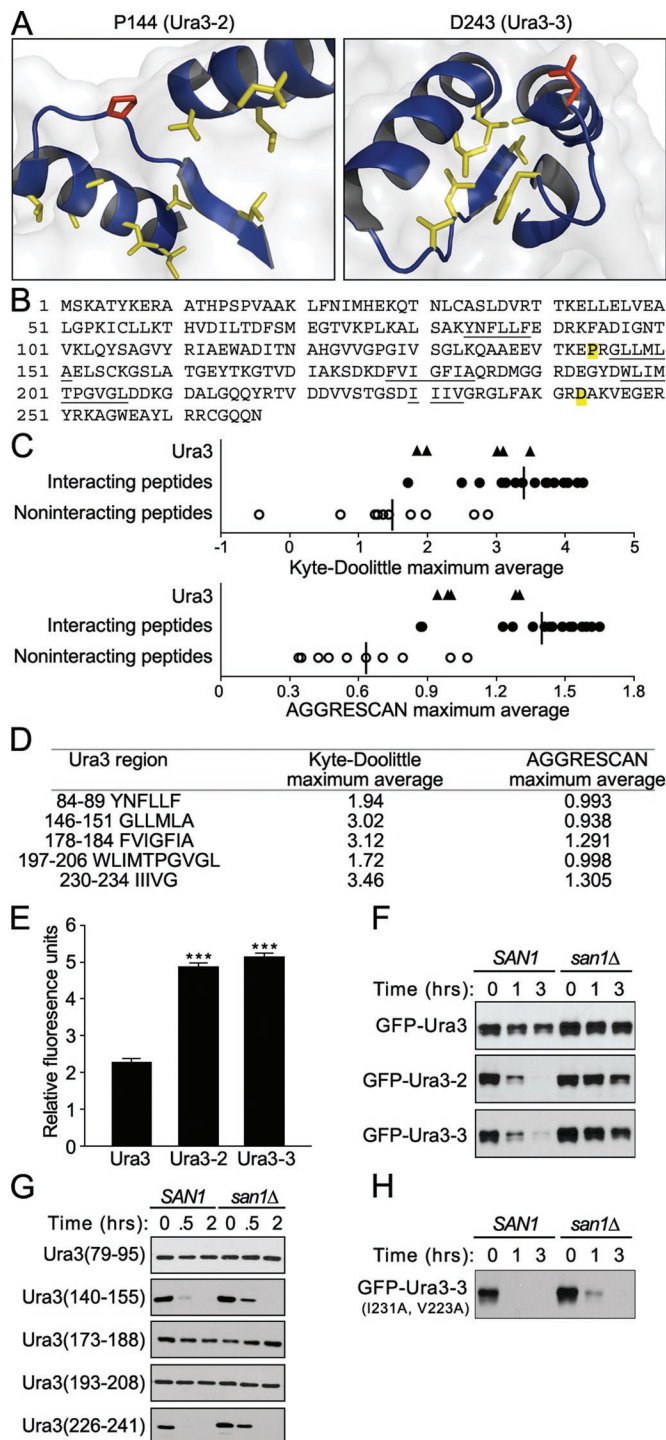
FIGURE 6: Missense Ura3 mutants have increased surface-exposed hydrophobicity in vitro that correlates with San1-dependent degradation in vivo. (A) Local regions in the structure of Ura3 that surround residues P144 and D243. Red indicates the residue that is mutated in each version of Ura3, and yellow indicates surrounding hydrophobic residues. Images were produced from PDB 3GDK using macPyMOL. (B) Sequence of Ura3. Mutated residues are highlighted in yellow, and structurally proximal hydrophobic regions are underlined. (C) K-D and AGGRESCAN sliding-scale analyses were performed to identify hydrophobic windows in Ura3 (▲). Shown are the regions with the top five maximum values. (D) The K-D and AGGRESCAN hydrophobic window values are listed for the Ura3 regions plotted in C. (E) Bacterially purified Ura3, Ura3-2, and Ura3-3 were incubated with 30 µM ANS for 1 h and fluorescence measured.

We tested this hypothesis using Rad16* (Figure 5), which confers toxicity when expressed in *san1Δ* cells (Figure 7A, Rad16*). Deletion of the hydrophobic region in Rad16* ameliorates its toxicity (Figure 7A, Rad16*Δh), linking exposed hydrophobicity to the detrimental effects of Rad16* expression. Using AGGRESCAN, we found that the Rad16* hydrophobic region is an aggregation "hot spot" (Figure 7B). Concordant with this prediction, Rad16*-GFP forms an inclusion body in the cytoplasm of wild-type *SAN1* cells but is absent from the nucleus due to San1-mediated degradation (Figure 7C, Rad16*-GFP). In *san1Δ* cells, Rad16*-GFP additionally accumulates throughout the nucleus and in a nuclear inclusion. Because Rad16* is toxic only in *san1Δ* cells (Figure 7A), we concluded that it is the nuclear pool of Rad16* that confers toxicity, not the cytoplasmic pool. Deletion of the hydrophobic region in Rad16* results in uniform cytoplasmic and predominantly nuclear localization in both wild-type and *san1Δ* cells, with no observable inclusion formation (Figure 7C, Rad16*Δh). Thus the hydrophobic region in Rad16* targeted by San1 is responsible for both Rad16* aggregation and toxicity when present in the nucleus. In other words, San1 targets the very abnormal feature in a misfolded protein that can cause aggregation and toxicity.

DISCUSSION

For effective PQC degradation to occur in the cell, PQC ubiquitin ligases must target a feature of structural abnormality that is commonly shared among many divergent misfolded proteins. Our analysis of the yeast nuclear PQC ubiquitin ligase San1 indicates that exposed hydrophobicity is the feature San1 recognizes in its disparate substrates, with a window of five contiguous hydrophobic residues defining the minimum amount of exposed hydrophobicity required for San1-mediated degradation. To determine how common this feature is among yeast proteins, we used the PatMatch tool in the *Saccharomyces cerevisiae* database (http://www.yeastgenome.org/cgi-bin/PATMATCH/nph-patmatch). The search identified 31,583 instances of five contiguous hydrophobic residues in 2471 of 5885 proteins (42% of the queried proteins), demonstrating that this feature is very common in the yeast proteome. It is reasonable to assume that the vast majority of these hydrophobic stretches are normally buried in a protein's core, at a protein–protein interface, or within a membrane environment and that their exposure would signify a defect in folding, assembly, or membrane insertion.

The San1-interacting and noninteracting peptides (Figure 1) show statistically significant differences in the means of their five-residue maximum sliding window K-D and AGGRESCAN hydrophobicity values (Figure 4). There was some overlap, however, in the range of values for San1-interacting peptides and noninteracting peptides. In particular, San1-interacting peptides 1 and G have maximum window values that fall within the range observed for the noninteracting peptides (Figure 4). Two possibilities might explain this overlap. First, the K-D and AGGRESCAN scores are likely to be reasonably good but not completely accurate measures of a

(F) Cycloheximide-chase assays were performed to assess the stability of the indicated GFP-Ura3 fusion in the presence or absence of *SAN1*. Time after cycloheximide addition is indicated above each lane. (G) Cycloheximide-chase assays were performed to assess the stability of the indicated GFP^{NLS}-Ura3 peptide fusion in the presence or absence of *SAN1*. Time after cycloheximide addition is indicated. (H) Cycloheximide-chase assay was performed to assess the stability of GFP^{NLS}–Ura3-3$^{I231A, V232A}$ fusion in the presence or absence of *SAN1*. Time after cycloheximide addition is indicated.
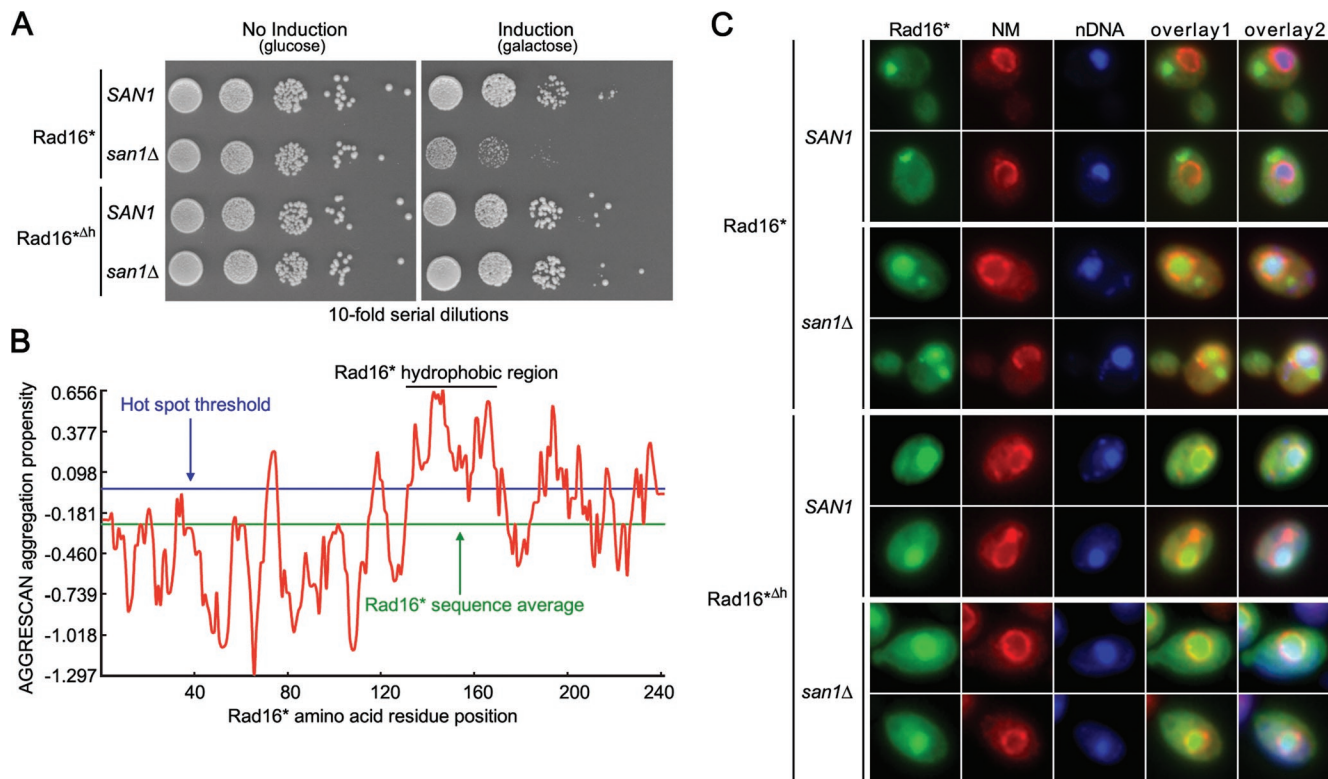
FIGURE 7: Nuclear aggregation and toxicity of Rad16* requires its hydrophobic patch. (A) *SAN1* or *san1Δ* cells expressing either Rad16* or Rad16*[Δh] were spotted onto media containing glucose to measure spotting efficiency or galactose to induce expression. (B) AGGRESCAN prediction of Rad16*. Regions above the blue threshold are considered aggregation prone. (C) Expression of GFP-tagged Rad16* or Rad16*[Δh] was induced in *SAN1* and *san1Δ* cells by growth in galactose for 8 h. Left, GFP fluorescence; middle, nuclear membrane (NM) visualized by a Dbp5-DsRed fusion and nuclear DNA (nDNA) visualized by staining with DAPI; right, overlays of the previous panels.
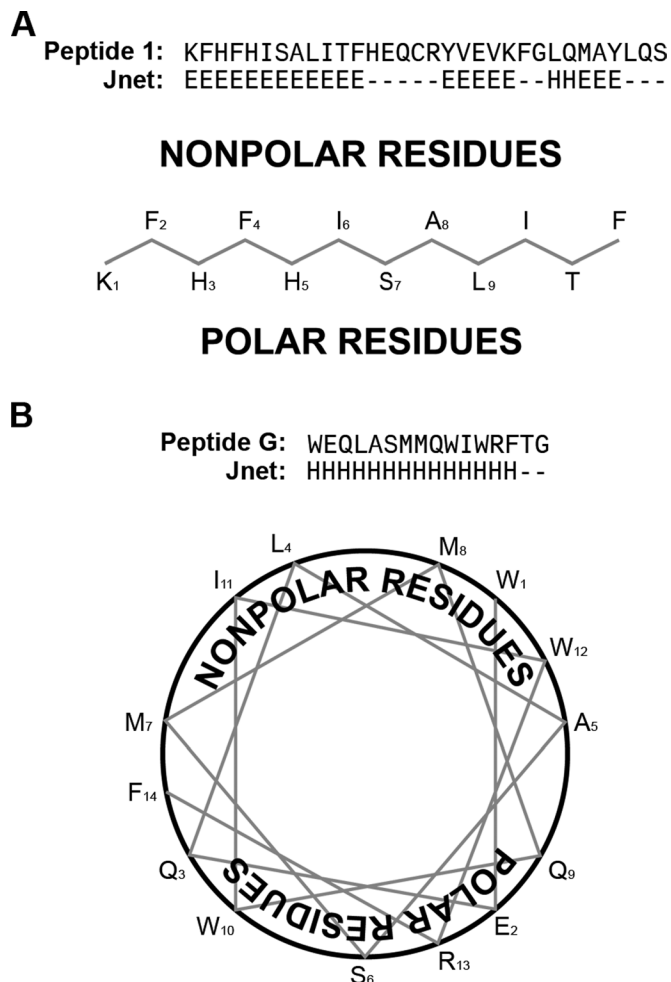
residue's hydrophobicity as it relates to San1 recognition. Each measure has its own biases in terms of assigning hydrophobicity values to residues, and we expect that these biases can result in underestimated maximum window values for some San1-interacting peptides (or possibly inflated maximum window values for some noninteracting peptides). Second, neither measure takes into account secondary structure. If a linear stretch of sequence forms an amphipathic α-helix or β-strand with hydrophobicity concentrated on one side of the secondary structure element, the peptide would not have a high maximum window value by either measure. In fact, using the JPRED 3 secondary structure predictor (Cole *et al.*, 2008), we find that peptide 1 is predicted to form an amphipathic β-strand and peptide G is predicted to form an amphipathic α-helix (Figure 8).

Two of the random peptides, L and Q, possess maximum window values that are in the range of the San1-interacting peptides, but neither peptide interacts with San1 in the two-hybrid assay. There are two possibilities why this might occur. The first is that these peptides are recognized by San1 but are also degraded by additional PQC degradation systems. In this scenario, the degradation of the GAD-peptide fusions would prevent acquisition of a sufficient steady-state level to trigger the two-hybrid interaction with San1. Consistent with this, both peptides are degraded primarily in a San1-independent manner. The second possibility is that the K-D and AGGRESCAN measures used to evaluate the maximum window of hydrophobicity do not take into account different types of hydrophobicity. Quite of interest, most of the San1-interacting peptides contain stretches of primarily valines, isoleucines, and leucines

(as do the stretches of hydrophobicity targeted by San1 in Rad16*, Sed1*, and Ura3), whereas peptides L and Q contain few of these residues (Figure 1). Perhaps San1 preferentially targets regions populated by high concentrations of branched-chain hydrophobic residues while disfavoring regions enriched with other types of hydrophobic residues. Future detailed studies will be required to determine the exact molecular rules that govern San1's hydrophobicity recognition preference.

In considering what misfolding means in the context of the Ura3 missense mutants, it is probable that overall secondary structures, including amphipathic ones, will remain relatively intact while their positioning in the Ura3 tertiary structure becomes disrupted. In support of this, a recent mutational study was undertaken to probe the folding kinetics of the PDZ domain from the D1 C-terminal processing protease (D1p) of *Scenedesmus obliquus* (Gianni *et al.*, 2010). Of interest, 10 of 40 different point mutations were found to trap the D1pPDZ domain in a common misfolded intermediate, which possesses nearly the same overall secondary structure content as the native protein, but the positions of its secondary structure elements are perturbed in its tertiary structure. By comparing the solvent-exposed surface area in the structure of the native protein with that of the misfolded intermediate, it was also found that the misfolded intermediate displays substantial surface exposure of hydrophobic regions that are normally buried in the native structure and distal to the mutations. This result mirrors that for the Ura3 missense mutant proteins that we used in this study, in which we observed increased surface hydrophobicity of the mutant proteins by ANS fluorescence in vitro. Definitive conclusions as to what San1 actually recognizes in

A

Peptide 1: `KFHFHISALITFHEQCRYVEVKFGLQMAYLQS`
Jnet: `EEEEEEEEEEEE-----EEEEE--HHEEE---`

NONPOLAR RESIDUES

POLAR RESIDUES

B

Peptide G: `WEQLASMMQWIWRFTG`
Jnet: `HHHHHHHHHHHHHHH--`

FIGURE 8: Secondary structure predictions of peptide 1 and peptide G. (A) JPRED 3 prediction (http://www.compbio.dundee.ac.uk/www-jpred/) of peptide 1's secondary structure and cartoon of peptide 1 residues' predicted positions in a β-strand. (B) JPRED 3 prediction of peptide G's secondary structure and helical wheel cartoon of peptide G residues' predicted positions in an α-helix.

the Ura3 mutants must await detailed structural studies of the mutants, but the results presented here are consistent with the hypothesis that San1 recognizes exposed hydrophobicity in misfolded missense mutant proteins.

The small window of hydrophobicity that San1 recognizes (window of five) is similar to the small window of hydrophobicity that Hsp70 chaperones bind in their client proteins (window of four) (Rudiger *et al.*, 1997). Hsp70 chaperones use a single, structurally well-defined, substrate-binding cleft to bind this window of hydrophobicity (Zhu *et al.*, 1996), whereas San1 appears to use multiple substrate-binding modules embedded within intrinsically disordered domains (Rosenbaum *et al.*, 2011). Given these different binding modalities, we believe that the similarity in exposed hydrophobicity targeted by San1 and Hsp70 chaperones provides an interesting example of convergent evolution by distinct PQC systems. The similarity raises a number of questions regarding the hierarchy of PQC decision making in the nucleus. Is there any coordination between San1 and chaperones, or do they simply compete for substrates? How is the balance of chaperone-facilitated refolding versus San1-mediated destruction regulated and optimized in the nucleus?

In the case of Rad16*, the hydrophobic region that San1 targets is also responsible for toxicity and aggregation. This underscores the functional purpose of PQC degradation systems like San1—to recognize structural abnormalities within misfolded proteins that can harm the cell. It is well established that exposed hydrophobicity can lead to deleterious protein aggregation (Chiti, 2006). The nucleus in particular is highly susceptible to aggregation, as evidenced by the many human disorders associated with nuclear aggregation (Woulfe, 2007). From an evolutionary perspective, it is not surprising then that exposed hydrophobicity is the specific structural abnormality recognized by San1. Although we have yet to identify a human San1 homologue, the human proteins PML IV and UHRF-2 have been implicated as potential nuclear PQC degradation ubiquitin ligases (Fu *et al.*, 2005; Janer *et al.*, 2006; Iwata *et al.*, 2009). Understanding what San1 and other nuclear PQC ubiquitin ligases recognize should provide new insights into why certain misfolded proteins escape nuclear PQC surveillance, accumulate, and cause cellular dysfunction.

MATERIALS AND METHODS
Yeast strains
Yeast strains used in this study are PJ69-4A (P$_{GAL2}$-ADE2, met2::P$_{GAL7}$-lacZ, his3Δ200, ura3–52, trp1–901, LYS::P$_{GAL1}$-HIS3, leu2–3112, gal4Δ, gal80Δ) (James *et al.*, 1996), BY4741 (met15Δ0, his3Δ1, ura3Δ0, leu2Δ0) (Brachmann *et al.*, 1998), RGY506 (BY4741 san1Δ), RGY1269 (his3Δ1, ura3Δ0, lys2Δ0, leu2Δ0, DBP5-dsRED::HIS3), and RGY1273 (RGY1269 san1Δ). Standard yeast media and yeast genetic methods were used (Guthrie and Fink, 1991).

Plasmids used in this study
Plasmids used in this study are listed in Supplemental Table S1. Plasmids were constructed using standard cloning protocols. The relevant coding regions of each construct used in this study were sequenced. Exact oligonucleotide sequences and plasmid construction details will be provided upon request.

Two-hybrid assays
Two-hybrid tests were performed as previously described (Rosenbaum *et al.*, 2011). Cells expressing GBD-San1^{C279S} and the appropriate GAD fusions were spotted onto selective (media minus histidine) and nonselective media (media plus histidine) to assess interactions and spotting efficiency. Identical strains expressing GBD-Ubp10 and the appropriate GAD fusions were tested as a control experiment. All interaction tests were performed in duplicate using two independent isolates. Growth plates were scanned on an Epson (Long Beach, CA) Perfection V350 Photo Scanner. Images were cropped and processed using the Mac version of Photoshop CS (Adobe, San Jose, CA).

Degradation assays
Cycloheximide-chase degradation assays were performed similar to those previously described (Gardner *et al.*, 2005). Cells were grown in synthetic media with 3% raffinose to ~1×10^7 cells/ml. Galactose was added to 3% and the cells incubated 2 h. Cycloheximide was added to 50 μg/ml and the cells further incubated for 0–5 h. Cells were lysed at the appropriate time point in 200 μl of SUMEB buffer (8 M urea, 1% SDS, 10 mM 3-(N-morpholino)propanesulfonic acid, pH 6.8, 10 mM EDTA, 0.01% bromophenol blue) by vortexing with 100 μl of 0.5-mm glass beads (BioSpec Products, Bartlesville, OK). Proteins were resolved on 8–16% SDS–PAGE gels, transferred to nitrocellulose, and immunoblotted with anti-GFP (Sigma-Aldrich, St. Louis, MO) antibodies in 2% milk. Blots were scanned on an Epson

Perfection V350 Photo Scanner. Images were cropped and processed using the Mac version of Photoshop CS.

Sliding window analysis

K-D and AGGRESCAN hydrophobicity values for each peptide tested were measured using a five-residue moving window. The maximum values recorded for each peptide were grouped according to that peptide's ability to interact with San1 by two-hybrid test. Interacting and noninteracting groups were evaluated by normal quantile plot, and both conformed to normal distributions. However, the sample groups had unequal sample sizes and variances. Therefore we compared the means for interacting and noninteracting groups using Welch's unpaired t test. One-tailed P values are reported because we are testing the hypothesis that San1-interacting peptides are more hydrophobic than noninteracting peptides.

In vitro hydrophobic binding assay

Plasmid DNA coding for Ura3, Ura3-2, and Ura3-3 6His fusions (see plasmid list) was transformed into T7 express cells (New England Biolabs, Ipswich, MA). Cells were grown in lysogeny broth (LB) with chloramphenicol at 37°C until an OD_{600} of ~1.0 was reached. Protein expression was induced by adding isopropyl β-D-1-thiogalactopyranoside (Gold Biotechnology, St. Louis, MO) to a final concentration of 300 μM, followed by incubation at 16°C overnight. Harvested cells were lysed in 10 ml of BugBuster (Novagen, EMD Biosciences, San Diego, CA) with 10 mM of phenylmethylsulfonyl fluoride. Soluble extract was applied to TALON resin (Novagen) equilibrated in a 300 mM NaCl, 50 mM Na_2HPO_4, pH 7.0 buffer. The column was washed with 7.5 mM imidazole (Sigma-Aldrich) added to the equilibration buffer, and protein was eluted with 150 mM imidazole. Forty microliters of 0.6 mg/ml recombinant protein and 10 μl of varying concentrations of ANS (Acros Organics, Geel, Belgium) were mixed in a 96-well plate and incubated at 25°C for 1 h. ANS fluorescence was excited at 375 nm, and absorbance measurements were taken at 485 nm. All ANS assays were conducted in triplicate.

Microscopy

Fixation and 4',6-diamidino-2-phenylindole (DAPI) staining of cells were performed as previously described (Gardner et al., 2005). Cells expressing GFP(S65T) or DsRED fusion proteins were grown in synthetic media with 3% raffinose to ~1 × 10⁷ cells/ml. Galactose was added to 3% and the cells incubated 8 h. Cells were fixed for 15 min in 4% paraformaldehyde. Fixed cells were washed and resuspended in potassium phosphate buffer (1.2 M sorbitol, 100 mM potassium phosphate, pH 7.5). Cells were then permeabilized by addition of 2% (vol/vol) Triton X-100 and stained for 1 min with the blue nucleic acid–binding dye DAPI (Molecular Probes, Invitrogen, Carlsbad, CA). Following staining, cells were washed and resuspended in potassium phosphate buffer. Fixed and stained cells were visualized at room temperature on a Nikon Eclipse E600 microscope (Nikon, Melville, NY) equipped with a 60× oil immersion objective, a 100-W mercury lamp, and filter sets to visualize GFP (FITC-HYQ), DsRED (Texas red-HYQ), and DAPI (UV-2A). Images were captured with a Photometrics CoolSNAP fx, 12-bit, cooled CCD camera (Photometrics, Tucson, AZ) and the accompanying RS Image software. All images were cropped and processed for publication using the Mac version of Photoshop CS.

REFERENCES

Addinall SG et al. (2008). A genomewide suppressor and enhancer analysis of cdc13-1 reveals varied cellular processes influencing telomere capping in Saccharomyces cerevisiae. Genetics 180, 2251–2266.

Betting J, Seufert W (1996). A yeast Ubc9 mutant protein with temperature-sensitive in vivo function is subject to conditional proteolysis by a ubiquitin- and proteasome-dependent pathway. J Biol Chem 271, 25790–25796.

Bhamidipati A, Denic V, Quan EM, Weissman JS (2005). Exploration of the topological requirements of ERAD identifies Yos9p as a lectin sensor of misfolded glycoproteins in the ER lumen. Mol Cell 19, 741–751.

Biederer T, Volkwein C, Sommer T (1996). Degradation of subunits of the Sec61p complex, an integral component of the ER membrane, by the ubiquitin-proteasome pathway. EMBO J 15, 2069–2076.

Bordallo J, Plemper RK, Finger A, Wolf DH (1998). Der3p/Hrd1p is required for endoplasmic reticulum-associated degradation of misfolded lumenal and integral membrane proteins. Mol Biol Cell 9, 209–222.

Brachmann CB, Davies A, Cost GJ, Caputo E, Li J, Hieter P, Boeke JD (1998). Designer deletion strains derived from Saccharomyces cerevisiae S288C: a useful set of strains and plasmids for PCR-mediated gene disruption and other applications. Yeast 14, 115–132.

Brodsky JL, Werner ED, Dubas ME, Goeckeler JL, Kruse KB, McCracken AA (1999). The requirement for molecular chaperones during endoplasmic reticulum-associated protein degradation demonstrates that protein export and import are mechanistically distinct. J Biol Chem 274, 3453–3460.

Buschhorn BA, Kostova Z, Medicherla B, Wolf DH (2004). A genome-wide screen identifies Yos9p as essential for ER-associated degradation of glycoproteins. FEBS Lett 577, 422–426.

Carvalho P, Goder V, Rapoport TA (2006). Distinct ubiquitin-ligase complexes define convergent pathways for the degradation of ER proteins. Cell 126, 361–373.

Chan KK, Wood BM, Fedorov AA, Fedorov EV, Imker HJ, Amyes TL, Richard JP, Almo SC, Gerlt JA (2009). Mechanism of the orotidine 5'-monophosphate decarboxylase-catalyzed reaction: evidence for substrate destabilization. Biochemistry 48, 5518–5531.

Chiti F (2006). Relative importance of hydrophobicity, net charge, and secondary structure propensities in protein aggregation. In: Protein Misfolding, Aggregation, and Conformational Diseases. Part A: Protein Aggregation and Conformational Diseases, Protein Reviews, Vol. 4, ed. VN Uversky, AL Fink, New York: Springer, 43–59.

Christianson JC, Shaler TA, Tyler RE, Kopito RR (2008). OS-9 and GRP94 deliver mutant alpha1-antitrypsin to the Hrd1-SEL1L ubiquitin ligase complex for ERAD. Nat Cell Biol 10, 272–282.

Clerc S, Hirsch C, Oggier DM, Deprez P, Jakob C, Sommer T, Aebi M (2009). Htm1 protein generates the N-glycan signal for glycoprotein degradation in the endoplasmic reticulum. J Cell Biol 184, 159–172.

Cole C, Barber JD, Barton GJ (2008). The JPRED 3 secondary structure prediction server. Nucleic Acids Res 36, 197–201.

Conchillo-Sole O, de Groot NS, Aviles FX, Vendrell J, Daura X, Ventura S (2007). AGGRESCAN: a server for the prediction and evaluation of "hot spots" of aggregation in polypeptides. BMC Bioinformatics 8, 65.

Dasgupta A, Ramsey KL, Smith JS, Auble DT (2004). Sir antagonist 1 (San1) is a ubiquitin ligase. J Biol Chem 279, 26830–26838.

Denic V, Quan EM, Weissman JS (2006). A luminal surveillance complex that selects misfolded glycoproteins for ER-associated degradation. Cell 126, 349–359.

Estruch F, Peiro-Chova L, Gomez-Navarro N, Durban J, Hodge C, Del Olmo M, Cole CN (2009). A genetic screen in Saccharomyces cerevisiae identifies new genes that interact with mex67-5, a temperature-sensitive allele of the gene encoding the mRNA export receptor. Mol Genet Genomics 281, 125–134.

Evans DR, Brewster NK, Xu Q, Rowley A, Altheim BA, Johnston GC, Singer RA (1998). The yeast protein complex containing cdc68 and pob3

mediates core-promoter repression through the cdc68 N-terminal domain. Genetics 150, 1393–1405.

Fang S, Ferrone M, Yang C, Jensen JP, Tiwari S, Weissman AM (2001). The tumor autocrine motility factor receptor, gp78, is a ubiquitin protein ligase implicated in degradation from the endoplasmic reticulum. Proc Natl Acad Sci USA 98, 14422–14427.

Fu L, Gao YS, Tousson A, Shah A, Chen TL, Vertel BM, Sztul E (2005). Nuclear aggresomes form by fusion of PML-associated aggregates. Mol Biol Cell 16, 4905–4917.

Gardner RG, Nelson ZW, Gottschling DE (2005). Degradation-mediated protein quality control in the nucleus. Cell 120, 803–815.

Gardner RG, Swarbrick GM, Bays NW, Cronin SR, Wilhovsky S, Seelig L, Kim C, Hampton RY (2000). Endoplasmic reticulum degradation requires lumen to cytosol signaling. Transmembrane control of Hrd1p by Hrd3p. J Cell Biol 151, 69–82.

Gauss R, Jarosch E, Sommer T, Hirsch C (2006). A complex of Yos9p and the HRD ligase integrates endoplasmic reticulum quality control into the degradation machinery. Nat Cell Biol 8, 849–854.

Gianni S, Ivarsson Y, De Simone A, Travaglini-Allocatelli C, Brunori M, Vendruscolo M (2010). Structural characterization of a misfolded intermediate populated during the folding process of a PDZ domain. Nat Struct Mol Biol 17, 1431–1437.

Gilon T, Chomsky O, Kulka RG (1998). Degradation signals for ubiquitin system proteolysis in *Saccharomyces cerevisiae*. EMBO J 17, 2759–2766.

Gilon T, Chomsky O, Kulka RG (2000). Degradation signals recognized by the Ubc6p-Ubc7p ubiquitin-conjugating enzyme pair. Mol Cell Biol 20, 7214–7219.

Guthrie C, Fink GR (1991). Guide to yeast genetics and molecular biology. Methods Enzymol 194, 1–863.

Hampton RY, Gardner RG, Rine J (1996). Role of 26S proteasome and HRD genes in the degradation of 3-hydroxy-3-methylglutaryl-CoA reductase, an integral endoplasmic reticulum membrane protein. Mol Biol Cell 7, 2029–2044.

Hawe A, Sutter M, Jiskoot W (2008). Extrinsic fluorescent dyes as tools for protein characterization. Pharm Res 25, 1487–1499.

Heck JW, Cheung SK, Hampton RY (2010). Cytoplasmic protein quality control degradation mediated by parallel actions of the E3 ubiquitin ligases Ubr1 and San1. Proc Natl Acad Sci USA 107, 1106–1111.

Hosokawa N, You Z, Tremblay LO, Nagata K, Herscovics A (2007). Stimulation of ERAD of misfolded null Hong Kong alpha1-antitrypsin by Golgi alpha1,2-mannosidases. Biochem Biophys Res Commun 362, 626–632.

Huyer G, Piluek WF, Fansler Z, Kreft SG, Hochstrasser M, Brodsky JL, Michaelis S (2004). Distinct machinery is required in *Saccharomyces cerevisiae* for the endoplasmic reticulum-associated degradation of a multispanning membrane protein and a soluble luminal protein. J Biol Chem 279, 38369–38378.

Iwata A, Nagashima Y, Matsumoto L, Suzuki T, Yamanaka T, Date H, Deoka K, Nukina N, Tsuji S (2009). Intra-nuclear degradation of polyglutamine aggregates by the ubiquitin proteasome system. J Biol Chem 284, 9796–9803.

James P, Halladay J, Craig EA (1996). Genomic libraries and a host strain designed for highly efficient two-hybrid selection in yeast. Genetics 144, 1425–1436.

Janer A, Martin E, Muriel MP, Latouche M, Fujigasaki H, Ruberg M, Brice A, Trottier Y, Sittler A (2006). PML clastosomes prevent nuclear accumulation of mutant ataxin-7 and other polyglutamine proteins. J Cell Biol 174, 65–76.

Jiang J, Ballinger CA, Wu Y, Dai Q, Cyr DM, Hohfeld J, Patterson C (2001). CHIP is a U-box-dependent E3 ubiquitin ligase: identification of Hsc70 as a target for ubiquitylation. J Biol Chem 276, 42938–42944.

Johnson PR, Swanson R, Rakhilina L, Hochstrasser M (1998). Degradation signal masking by heterodimerization of MATalpha2 and MATa1 blocks their mutual destruction by the ubiquitin-proteasome pathway. Cell 94, 217–227.

Kaganovich D, Kopito R, Frydman J (2008). Misfolded proteins partition between two distinct quality control compartments. Nature 454, 1088–1095.

Kanehara K, Xie W, Ng DT (2010). Modularity of the Hrd1 ERAD complex underlies its diverse client range. J Cell Biol 188, 707–716.

Kaneko M, Ishiguro M, Niinuma Y, Uesugi M, Nomura Y (2002). Human HRD1 protects against ER stress-induced apoptosis through ER-associated degradation. FEBS Lett 532, 147–152.

Kim W, Spear ED, Ng DT (2005). Yos9p detects and targets misfolded glycoproteins for ER-associated degradation. Mol Cell 19, 753–764.

Kyte J, Doolittle RF (1982). A simple method for displaying the hydropathic character of a protein. J Mol Biol 157, 105–132.

Lewis MJ, Pelham HR (2009). Inefficient quality control of thermosensitive proteins on the plasma membrane. PLoS One 4, e5038.

Matsuo Y, Kishimoto H, Tanae K, Kitamura K, Katayama S, Kawamukai M (2011). Nuclear protein quality is regulated by the ubiquitin-proteasome system through the activity of Ubc4 and San1 in fission yeast. J Biol Chem. 286, 13775–13790.

McClellan AJ, Scott MD, Frydman J (2005). Folding and quality control of the VHL tumor suppressor proceed through distinct chaperone pathways. Cell 121, 739–748.

McDonough H, Patterson C (2003). CHIP: a link between the chaperone and proteasome systems. Cell Stress Chaperones 8, 303–308.

Metzger MB, Maurer MJ, Dancy BM, Michaelis S (2008). Degradation of a cytosolic protein requires endoplasmic reticulum-associated degradation machinery. J Biol Chem 283, 32302–32316.

Mijaljica D, Prescott M, Devenish RJ (2007). Nibbling within the nucleus: turnover of nuclear contents. Cell Mol Life Sci 64, 581–588.

Mueller B, Lilley BN, Ploegh HL (2006). SEL1L, the homologue of yeast Hrd3p, is involved in protein dislocation from the mammalian ER. J Cell Biol 175, 261–270.

Murata S, Minami Y, Minami M, Chiba T, Tanaka K (2001). CHIP is a chaperone-dependent E3 ligase that ubiquitylates unfolded protein. EMBO Rep 2, 1133–1138.

Nadav E, Shmueli A, Barr H, Gonen H, Ciechanover A, Reiss Y (2003). A novel mammalian endoplasmic reticulum ubiquitin ligase homologous to the yeast Hrd1. Biochem Biophys Res Commun 303, 91–97.

Nakatsukasa K, Huyer G, Michaelis S, Brodsky JL (2008). Dissecting the ER-associated degradation of a misfolded polytopic membrane protein. Cell 132, 101–112.

Nillegoda NB, Theodoraki MA, Mandal AK, Mayo KJ, Ren HY, Sultana R, Wu K, Johnson J, Cyr DM, Caplan AJ (2010). Ubr1 and Ubr2 function in a quality control pathway for degradation of unfolded cytosolic proteins. Mol Biol Cell 21, 2102–2116.

Park SH, Bolender N, Eisele F, Kostova Z, Takeuchi J, Coffino P, Wolf DH (2007). The cytoplasmic Hsp70 chaperone machinery subjects misfolded and endoplasmic reticulum import-incompetent proteins to degradation via the ubiquitin-proteasome system. Mol Biol Cell 18, 153–165.

Quan EM, Kamiya Y, Kamiya D, Denic V, Weibezahn J, Kato K, Weissman JS (2008). Defining the glycan destruction signal for endoplasmic reticulum-associated degradation. Mol Cell 32, 870–877.

Ravid T, Kreft SG, Hochstrasser M (2006). Membrane and soluble substrates of the Doa10 ubiquitin ligase are degraded by distinct pathways. EMBO J 25, 533–543.

Rosenbaum JC *et al.* (2011). Disorder targets misorder in nuclear quality control degradation: a disordered ubiquitin ligase directly recognizes its misfolded substrates. Mol Cell 41, 93–106.

Ross CA, Poirier MA (2005). Opinion: what is the role of protein aggregation in neurodegeneration? Nat Rev Mol Cell Biol 6, 891–898.

Rudiger S, Germeroth L, Schneider-Mergener J, Bukau B (1997). Substrate specificity of the DnaK chaperone determined by screening cellulose-bound peptide libraries. EMBO J 16, 1501–1507.

Sadis S, Atienza C Jr, Finley D (1995). Synthetic signals for ubiquitin-dependent proteolysis. Mol Cell Biol 15, 4086–4094.

Sato BK, Schulz D, Do PH, Hampton RY (2009). Misfolded membrane proteins are specifically recognized by the transmembrane domain of the Hrd1p ubiquitin ligase. Mol Cell 34, 212–222.

Schnell R, D'Ari L, Foss M, Goodman D, Rine J (1989). Genetic and molecular characterization of suppressors of SIR4 mutations in *Saccharomyces cerevisiae*. Genetics 122, 29–46.

Skovronsky DM, Lee VM, Trojanowski JQ (2006). Neurodegenerative diseases: new concepts of pathogenesis and their therapeutic implications. Annu Rev Pathol 1, 151–170.

Swanson R, Locher M, Hochstrasser M (2001). A conserved ubiquitin ligase of the nuclear envelope/endoplasmic reticulum that functions in both ER-associated and Matalpha2 repressor degradation. Genes Dev 15, 2660–2674.

Taxis C, Hitt R, Park SH, Deak PM, Kostova Z, Wolf DH (2003). Use of modular substrates demonstrates mechanistic diversity and reveals differences in chaperone requirement of ERAD. J Biol Chem 278, 35903–35913.

Vashist S, Kim W, Belden WJ, Spear ED, Barlowe C, Ng DT (2001). Distinct retrieval and retention mechanisms are required for the quality control of endoplasmic reticulum protein folding. J Cell Biol 155, 355–368.

Vashist S, Ng DT (2004). Misfolded proteins are sorted by a sequential checkpoint mechanism of ER quality control. J Cell Biol 165, 41–52.

Vembar SS, Brodsky JL (2008). One step at a time: endoplasmic reticulum-associated degradation. Nat Rev Mol Cell Biol 9, 944–957.

Wang Z, Jones GM, Prelich G (2006). Genetic analysis connects SLX5 and SLX8 to the SUMO pathway in *Saccharomyces cerevisiae*. Genetics 172, 1499–1509.

Wang Z, Prelich G (2009). Quality control of a transcriptional regulator by SUMO-targeted degradation. Mol Cell Biol 29, 1694–1706.

Ward CL, Omura S, Kopito RR (1995). Degradation of CFTR by the ubiquitin-proteasome pathway. Cell 83, 121–127.

Wickner S, Maurizi MR, Gottesman S (1999). Posttranslational quality control: folding, refolding, and degrading proteins. Science 286, 1888–1893.

Woulfe JM (2007). Abnormalities of the nucleus and nuclear inclusions in neurodegenerative disease: a work in progress. Neuropathol Appl Neurobiol 33, 2–42.

Xie W, Kanehara K, Sayeed A, Ng DT (2009). Intrinsic conformational determinants signal protein misfolding to the Hrd1/Htm1 endo-plasmic reticulum-associated degradation system. Mol Biol Cell 20, 3317–3329.

Xu Q, Johnston GC, Singer RA (1993). The *Saccharomyces cerevisiae* Cdc68 transcription activator is antagonized by San1, a protein implicated in transcriptional silencing. Mol Cell Biol 13, 7553–7565.

Yang M, Wu Z, Fields S (1995). Protein-peptide interactions analyzed with the yeast two-hybrid system. Nucleic Acids Res 23, 1152–1156.

Zhu X, Zhao X, Burkholder WF, Gragerov A, Ogata CM, Gottesman ME, Hendrickson WA (1996). Structural analysis of substrate binding by the molecular chaperone DnaK. Science 272, 1606–1614.